Letter

Light-Induced Atomic Desorption in Microfabricated Vapor Cells for Demonstrating Quantum Optical Applications

Eliran Talker,[1] Pankaj Arora,[1] Roy Zektzer,[1] Yoel Sebbag,[1] Mark Dikopltsev,[1,2] and Uriel Levy[1,*]

[1] *Department of Applied Physics, The Faculty of Science, The Center for Nanoscience and Nanotechnology, The Hebrew University of Jerusalem, Jerusalem 91904, Israel*

[2] *RAFAEL, Science Center, Rafael Ltd., Haifa 31021, Israel*

(Received 7 January 2021; revised 5 March 2021; accepted 30 March 2021; published 6 May 2021)

In recent years, we have observed substantial efforts towards the miniaturization of atomic vapor cells from the centimeter scale down to the millimeter scale and even lower, to enable efficient and compact light-vapor interactions with a higher degree of integration, lower heating power, and other prominent advantages. However, miniaturization typically comes at the cost of a reduced optical path, effectively reducing the contrast of the optical signal. To overcome this obstacle, we perform light-induced atomic desorption (LIAD) on a microfabricated buffer-gas-filled vapor cell and significantly increase the contrast of the optical signal. LIAD is a nonthermal process, whereby atoms absorbed at a surface are released under nonresonant-light illumination. A compact on-chip atomic optical isolator at room temperature is presented using the LIAD technique in our millimeter-sized fabricated vapor cell. The use of LIAD is found to be an excellent option to realize a narrow-line-width optical isolator at room temperature. Furthermore, the LIAD technique is utilized to demonstrate dichroic atomic vapor laser lock (DAVLL) in the same microfabricated vapor cell without heating. Taking advantage of the LIAD-enhanced DAVLL signal in the miniaturized vapor cell, we stabilize a 780-nm laser with a precision better than 400 kHz, without the need for heating and with no frequency modulation. Eliminating the need for heating may pave the way for remote applications, where the cell may be far away from the lasers, in scenarios where electrical currents and electrical contacts are undesired and difficult to implement.

DOI: 10.1103/PhysRevApplied.15.L051001

I. INTRODUCTION

Atomic vapor cells are the basis for applications such as optical frequency reference [1–5], magnetic and electric field sensors [6–8], narrowband atomic filters [9,10], and magnetometers [11–13], to name a few. Recently, there has been much interest in small reliable chip-sized alkali-vapor cells [2,14]. However, while confining the atomic vapor in small geometries, the interaction length of light and vapor is significantly reduced, as a result of which, a reduction, in contrast, is observed in the optical signal. Moreover, additional effects need to be considered. For example, atom-surface interactions become more important because atomic polarization relaxes rapidly when atoms collide with cell walls [15–17]. In this regard, antirelaxation coatings [18,19] (e.g., paraffin) and the use of buffer gas [20,21] in vapor cells are applied to reduce the wall-collision relaxation rate.

One approach to enhance the contrast of the signal is by heating vapor in the cell, which consequently increases the atomic number density and the optical density. However, the increase in temperature is followed by a larger Doppler broadening [22,23]. Moreover, the heating is of limited use with paraffin-coated cells [18], because the performance of paraffin coatings quickly degrades at temperatures above 60–80 °C. In this regard, another possible route to increase the vapor density in miniaturized cells at room temperature is the use of the light-induced atomic desorption (LIAD) technique [24–27], where the atoms are desorbed from the surface of the vapor cell into the volume of the cell by exposing the cell to photons of sufficiently high energy and flux. In particular, the use of the LIAD technique is very useful when heating techniques are not suitable, such as in the case of paraffin-coated cells, which are largely used in miniaturized atomic clocks and magnetometers. The use of LIAD is expected to play a dominant role in miniaturized cells due to the higher surface-to-volume ratio.

In the recent past, the atomic vapor cell has been used to demonstrate optical isolation and dichroic atomic vapor laser lock (DAVLL), albeit at high temperatures and strong magnetic fields [28,29]. Here, we exploit the use of LIAD in a buffer-gas-filled microfabricated vapor cell to realize an atomic optical isolator at room temperature and with a magnetic field as low as 300 G. Furthermore, we demonstrate a stable locking signal with a compact microfabricated vapor cell, where the LIAD technique is

*ulevy@mail.huji.ac.il

utilized to increase the vapor density instead of heating the cell. This way, we stabilize a 780-nm laser to a precision better than 400 kHz without the need for heating and without using frequency modulation. The use of LIAD allows an increase in the signal-to-noise ratio by releasing atoms from the surface and increasing the atomic density, whereas the use of DAVLL allows the instability to be reduced because this scheme does not rely on modulation while locking the laser.

II. LIAD TECHNIQUE IN A MICROFABRICATED VAPOR CELL

To increase the vapor density without heating in the microfabricated vapor cell using the LIAD technique, several vapor cells of the same dimensions, but with different values of buffer-gas pressure, are used. The uncoated cell is fabricated using triple-stack anodic bonding [30] with a cell radius of 0.5 mm and a length of 2 mm. A diode laser (Toptica DL-Pro) of 780 nm in wavelength, a power of 0.2 mW, and a beam diameter of about 2 mm is used to scan across the ^{87}Rb D_2 transition ($5^2S_{1/2} \rightarrow 5^2P_{3/2}$). The light transmitted through the cell is captured by a photodetector. A 780-nm-wavelength bandpass filter is placed in front of the photodetector to avoid undesired light from arriving at it. To increase the atomic number density at room temperature using LIAD, the cell is uniformly illuminated by 365-nm-wavelength light from a light-emitting diode (LED) with an intensity of about 4 mW/cm^2. The use of UV LED light is the most efficient wavelength for the release of rubidium atoms from the surface [31]. The relationship between the wavelength chosen for the LIAD process and the specific atomic vapor can be described in analogy to the well-understood photoelectric effect [32]. The intensity of LED light is chosen to be 4 mW/cm^2 to avoid undesired processes, such as local heating due to high LED light intensities. The illumination is maintained constant for about 5 min, after which we begin to observe a small degradation in the absorption signal. To accommodate this effect, we then turn off the light for approximately 2 s and turn it on again until reaching maximum absorption. This process is repeated for the duration of the experiment. A thermistor is mounted on the outer wall of the cell to detect the change in cell temperature during the illumination process. Figures 1(a) and 1(b) show the captured transmission signal through cells filled with pure ^{87}Rb and a mixture of Ar and N_2 buffer gas (in a ratio of 2:1) of different pressure values. Upon illumination with UV light, an appreciable change in the contrast (pink region) of the transmission dips, corresponding to the D_2 transitions from the $F_g = 1$ and $F_g = 2$ ground levels, is observed. When the UV light is switched off, the vapor density in the cell quickly decays to equilibrium density (blue region). This on-off light cycle can be repeated at will and the same results are obtained. During exposure to UV light, the temperature of the cell is almost constant (a negligible change of about 1 °C is measured), and thus, the increase in atomic density can only be explained

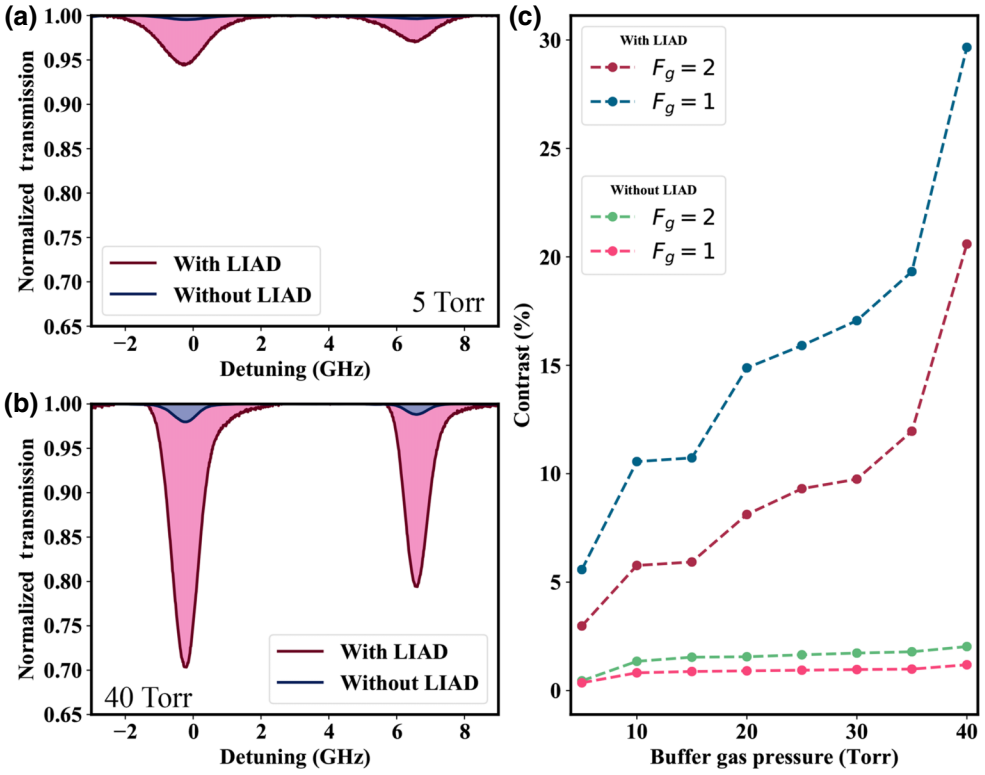

FIG. 1. Measured transmission signal through miniaturized vapor cells filled with (a) 5 Torr, and (b) 40 Torr of buffer-gas pressure. Measurements are made at room temperature. Significant increase in contrast after illuminating the vapor cell with blue light is easily observed. (c) Measured contrast of transmission signal as a function of buffer-gas pressure with and without LIAD; all measurements are done at room temperature (27 °C) using Earth's magnetic field (∼0.5 G) and linearly polarized light.

by the LIAD process and cannot be attributed to heating of the vapor cell. It is also observed that the transmission contrast can be drastically improved by increasing the buffer-gas pressure. This is expected from Beer-Lambert's law, as absorption is related to the vapor density of the cell, which is proportional to the square root of the buffer-gas pressure [33].

III. REALIZATION OF AN OPTICAL ISOLATOR USING LIAD

Next, after demonstrating the positive role of LIAD in increasing the vapor density within our miniaturized vapor cell, we move to demonstrate an optical isolator at room temperature using the experimental setup shown in Fig. 2(a). A 780-nm-wavelength laser beam with a power of 0.2 mW is scanned across the ^{87}Rb D_2 transition ($5S_{1/2} \rightarrow 5P_{3/2}$). After passing through a PBS, the output beam is linearly polarized along the horizontal direction and is incident on a millimeter-sized vapor cell containing pure ^{87}Rb and buffer gas with 40 Torr. The compactness of the cell makes it easy to maintain a uniform magnetic field across it by using small and inexpensive magnets as an alternative to current-carrying coils. An aluminum holder is used to hold the axially magnetized two-ring permanent magnets, allowing the laser beam to pass through. The distance between these two permanent magnets is adjusted to set the intensity of the magnetic field to a value of 300 G, as verified by a gauss meter (Lakeshore). Magnetization of the two magnets is chosen to be in the same direction, such that the magnets attract each other. Since the path of the laser in the Rb cell coincides with the central axis of the two permanent magnets, the magnetic field in the interaction area of the laser and the Rb atom can be considered as uniform. A second PBS is set to $\pi/4$ to allow high transmission, T_+, along the $+z$ direction and low transmission, T_-, along the $-z$ direction. The transmission spectrum is captured by a photodetector.

The mechanism of an optical isolator based on an atomic vapor cell, placed between two crossed linear polarizers, or polarized beam splitters [Fig. 2(a)], is fairly simple. When an external magnetic field is applied along the optical axis, the m_F levels split asymmetrically. The σ^+ and σ^- components of the linearly polarized light, now experience different phase shifts when passing through the medium; this results in a net rotation of the linearly polarized light. Using the principle of the Faraday effect, as shown in Fig. 2(a), a beam passes through the cell, where the magnetic field is applied parallel to the optical axis. The value of $\pi/4$ of the output polarizer with respect to the incident ensures high transmission along the positive z direction (T_+) for an induced polarization rotation of $\pi/4$. With this arrangement, one would also expect isolation along the negative z direction (T_-). An ideal isolator provides a $\pi/4$ polarization rotation alongside with minimal absorption. The angle of polarization rotation within the cell is

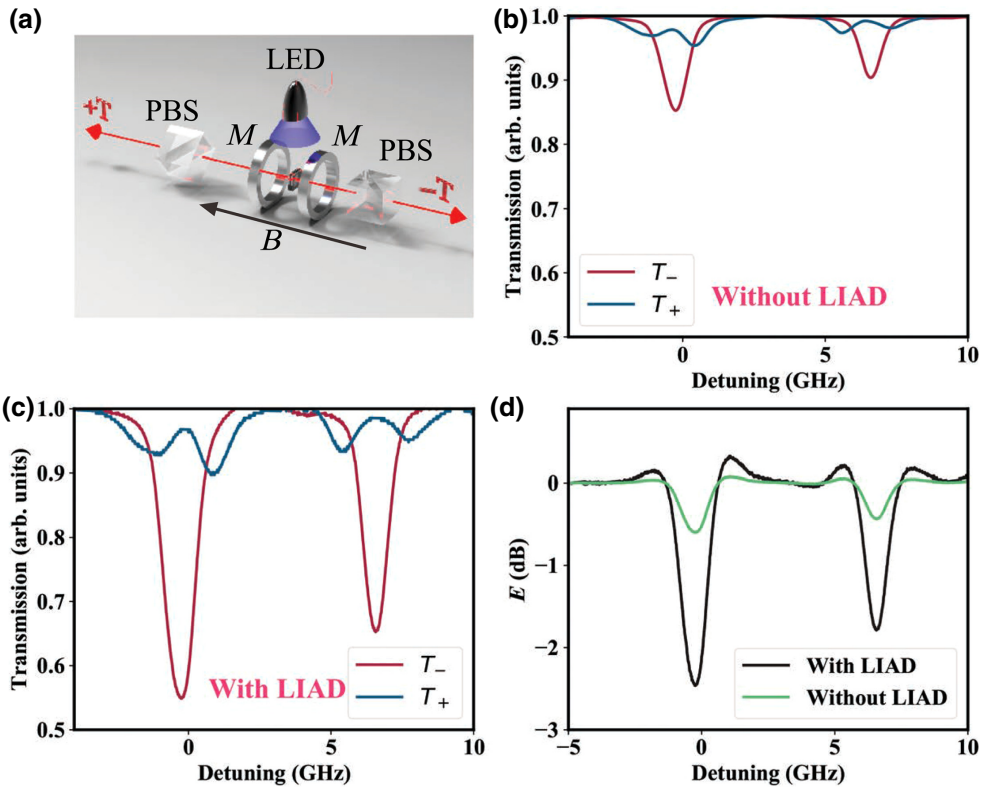

FIG. 2. (a) Experimental setup to realize an optical isolator in a millimeter-sized vapor cell; PBS, polarization beam splitter; *M*, magnets; LED, blue-light LED. All measurements are made at 40 °C using a cell with buffer-gas pressure of 40 Torr. Optical isolation as a function of laser detuning. Forward T_+ and backward T_- transmission signals illustrate optical isolator effect in vapor cell (b) without LIAD and (c) with LIAD. (d) Extinction value of isolation for realized optical isolator.

given by

$$\theta \approx nPL, \tag{1}$$

where L is the path length of the probe beam through the cell, n is the density of alkali atoms, and P is the polarization of the alkali vapor along the probe beam direction.

As can be seen from Eq. (1), increasing the density will increase the Faraday rotation. This can be achieved using the LIAD technique. To calculate the isolation ratio [$E = -\log_{10}(T_+/T_-)$ dB], the transmission spectra of the signals T_+ and T_-, propagating through the vapor cell filled with buffer gas at a pressure of 40 Torr, at a temperature of 40 °C, upon the application of a 300-G magnetic field, are plotted in Figs. 2(b)–2(c). Figure 2(d) shows the extracted extinction value of isolation. As can be seen, an isolation value of 3 dB is achieved at room temperature when LIAD is applied, in comparison to about 0.5 dB without LIAD. Previously reported isolators measure very good extinctions [10], but at a very high temperature (135 °C) and under a strong magnetic field (0.5 T). As previously discussed, high temperatures are typically less desired due to system and technological limitations, as well as the need to minimize broadening effects. Furthermore, while the use of an increased value of magnetic field (e.g., 0.5 T) with neodymium permanent magnets will increase the Faraday rotation angle and could improve the optical isolator performance, our final goal is to achieve a chip-scale optical isolator by fabricating the metal strip directly on the vapor cell, to realize a magnetic field value of about 300 G. The use of large permanent magnets to realize a high value of magnetic field will make the proposed device more cumbersome and is thus less desired for our purposes. Here, we propose a narrowband atomic vapor isolator realized at room temperature with a small value of magnetic field using the LIAD technique. The efficiency of the LIAD approach is enhanced for miniaturized cells, owing to the increase in surface-to-volume ratio. The extinction value of the realized isolator can be further improved by using several miniaturized cells in a back-to-back configuration and by using a stronger magnetic field, which will increase polarization of the atoms. We also show the effect of temperature on the realized optical isolator signal obtained with the LIAD technique (see Fig. S1 within the Supplemental Material [34]).

IV. LASER-FREQUENCY STABILIZATION WITH DAVLL SIGNAL USING LIAD

Finally, we demonstrate the effect of LIAD on improving laser-frequency stabilization. The development of laser-frequency-locking systems has been an active topic of research for many years. A simple laser-lock scheme, DAVLL, is a technique that relies upon the differential Doppler-broadened absorption signal of two orthogonal circular polarizations in atomic vapor in the presence of an external magnetic field. The magnitude of the applied magnetic field is set to provide Zeeman shifts that are comparable to the Doppler-broadened width of the absorption line, so that the resulting DAVLL signal permits the lock point to be tuned over a large range of frequencies. Another advantage of the DAVLL scheme is its simplicity and elimination of the need for external frequency modulation while locking the laser. In the past, DAVLL was demonstrated in small vapor cells with external heating to increase the vapor density in the cell [28]. Here, we eliminate the need for constant heating by using the LIAD technique to increase the atomic density.

A schematic of the experimental setup is shown in Fig. 3(a). A linearly polarized laser beam of 780 nm in wavelength is passed through the miniaturized atomic vapor cell. A half-wave plate in combination with the PBS is used to set the power and improve the polarization purity of the beam. After exiting the vapor cell, the beam is passed through a quarter-wave plate (at 45°) before impinging on another PBS. A pair of permanent magnets is used to apply a uniform magnetic field (300 G) to the vapor cell. Due to the presence of the magnetic field, the atomic medium becomes dichroic. The signals arriving at the detectors at the output of the second PBS correspond to the right and left circularly polarized beams. Due to the Zeeman shift, the center of the absorption line for one of the circularly polarized light components is displaced to a higher laser frequency, while the other absorption line is displaced to a lower frequency. As a result, the difference in readings of the two photodetectors has a dispersionlike shape, with zero around the central frequency [Fig. 3(b)]. The signals are detected with a balanced photodetector, which produces a difference signal. This difference (error) signal shown in Fig. 3(b) is used to regulate the frequency of the laser (see also Figs. S2 and S3 within the Supplemental Material [34]). To increase the atomic number density using LIAD, the cell is homogenously illuminated by 365-nm-wavelength LED light with an intensity of about 4 mW/cm^2.

To show the locking capabilities of our system, a 780-nm-wavelength laser is locked by feeding the obtained error signal to a PI system and supplying the correction signal to the laser wavelength control. Figure 3(c) shows the plotted error signal, which is converted from volts to frequency, over time as we turn on the PI system. An Allan deviation analysis is also performed for the laser stability when it is locked and when it is free running [Fig. 3(d)]. This is done by analyzing the error signal (the difference between the two photodetectors, which corresponds to the difference between the two orthogonal states of circularly polarized light) of the system when we lock it and when the laser is free running [Fig. 3(c)]. As shown, we can lock the laser with our system to a level of about 10^{-9} (400 kHz) at 1 s (red curve), which is an order of magnitude

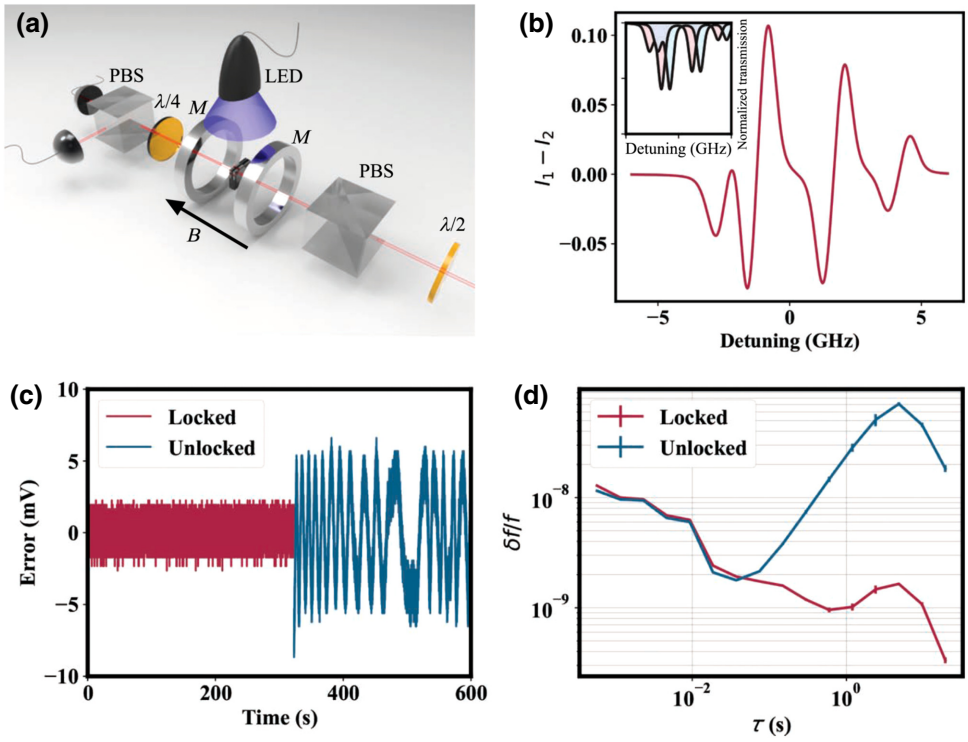

FIG. 3. (a) Experimental setup to realize DAVLL in miniaturized cell with LIAD technique. (b) Obtained error signal from transmission spectra of two orthogonal circularly polarized beams. Inset shows transmission spectra for left and right circularly polarized beams. (c) Measured error signal from system as a function of time. Red and blue lines represent cases when the proportional integral (PI) is off and on, respectively. (d) Allan deviation analysis of error signal. Blue and red lines correspond to free-running laser and locked laser, respectively.

improvement compared with the free-running laser (blue curve). It is important to mention that we measure only the correlation between our system and the laser, and therefore, the result represents a lower limit of frequency stability. A better estimate can be obtained in the future by comparing the signal to a reference system. The locking method shows a locking bandwidth in the order of several megahertz, after which the frequency noise averages to $1/\tau^{0.5}$ until it hits a flicker noise of about 3×10^{-10}. For white-noise-limited systems, frequency instability is known to be represented by the following expression: $\delta f/f = N/(QS)\tau^{-0.5}$, where Q is the Q factor of the absorption signal, N is the noise, S is the signal, and τ is the averaging time. The presented method of locking has a major advantage over the standard wavelength-modulation scheme because we can lock without modulating the laser frequency, which is an additional noise source. This, combined with the LIAD approach, which provides about a 3 times increase in contrast, benefits our system and makes it a promising method for room-temperature frequency references.

V. CONCLUSION

LIAD is applied to a miniaturized vapor cell. The efficiency of LIAD is enhanced for miniaturized cells, owing to the increase in surface-to-volume ratio. Following a demonstration of room-temperature atomic spectroscopy with LIAD-enhanced contrast, we utilize this approach to demonstrate a compact atomic optical isolator and laser-frequency stabilization. Both demonstrations are achieved at room temperature and with a magnetic field of about 300 G. Owing to the use of LIAD, an isolation extinction ratio of about 3 dB is achieved; in contrast to that of about 0.5 dB without LIAD. Laser stabilization is based on the DAVLL approach, eliminating the need for modulation. We can lock the laser to a level of about 10^{-9} (400 kHz) at 1 s and observe an order of magnitude improvement, compared with the free-running laser. Further work will focus on improving the extinction ratio of isolation and frequency stability. Finally, operating at room temperature with no heating may be of great importance in remote applications, where the cell is distant from lasers and the implementation of electrical currents and electrical contacts is challenging and undesired. In the future, we believe that, by using the LIAD platform in our vapor cells, it will be possible to observe quantum effects such as photon entanglement, where the increase in atom density is an important parameter that assists in observing such photon entanglement [35,36]. Furthermore, applications such as quantum magnetometry and quantum atomic clocks can also benefit from increasing the atomic density by obtaining a better signal-to-noise ratio.

ACKNOWLEDGMENTS

We acknowledge financial support from the Israeli Science Foundation. We thank Rafael Advanced Defense Systems (Israel) for their support in the preparation of buffer-gas-filled Rb vapor cells.

[1] S. Knappe, P. D. D. Schwindt, V. Gerginov, V. Shah, L. Liew, J. Moreland, H. G. Robinson, L. Hollberg, and J. Kitching, Microfabricated atomic clocks and magnetometers, J. Opt. A Pure Appl. Opt. **8**, S318 (2006).

[2] E. Talker, R. Zektzer, Y. Barash, N. Mazurski, and U. Levy, Atomic spectroscopy and laser frequency stabilization with scalable micrometer and Sub-micrometer vapor cells, J. Vac. Sci. Technol. B **38**, 050601 (2020).

[3] G. P. Barwood, P. Gill, and W. R. C. Rowley, A simple rubidium-stabilised laser diode for interferometric applications, J. Phys. E. **21**, 966 (1988).

[4] M. T. Hummon, S. Kang, D. G. Bopp, Q. Li, D. A. Westly, S. Kim, C. Fredrick, S. A. Diddams, K. Srinivasan, V. Aksyuk, and J. E. Kitching, Photonic chip for laser stabilization to an atomic vapor with 10^{-11} instability, Optica **5**, 443 (2018).

[5] S. T. Müller, D. V. Magalhães, R. F. Alves, and V. S. Bagnato, Compact frequency standard based on an intracavity sample of cold cesium atoms, J. Opt. Soc. Am. B **28**, 2592 (2011).

[6] H. Fan, S. Kumar, J. Sedlacek, H. Kübler, S. Karimkashi, and J. P. Shaffer, Atom based RF electric field sensing, J. Phys. B At. Mol. Opt. Phys. **48**, 202001 (2015).

[7] A. Horsley, G.-X. Du, and P. Treutlein, Widefield microwave imaging in alkali vapor cells with Sub-100 μm resolution, New J. Phys. **17**, 112002 (2015).

[8] A. Horsley, G. X. Du, M. Pellaton, C. Affolderbach, G. Mileti, and P. Treutlein, Imaging of relaxation times and microwave field strength in a microfabricated vapor cell, Phys. Rev. A - At. Mol. Opt. Phys. **88**, 1 (2013).

[9] E. Talker, P. Arora, M. Dikopoltsev, and U. Levy, Optical isolator based on highly efficient optical pumping of Rb atoms in a miniaturized vapor cell, J. Phys. B At. Mol. Opt. Phys. **53**, 045201 (2020).

[10] L. Weller, K. S. Kleinbach, M. A. Zentile, S. Knappe, I. G. Hughes, and C. S. Adams, Optical isolator using an atomic vapor in the hyperfine paschen–back regime, Opt. Lett. **37**, 3405 (2012).

[11] I. K. Kominis, T. W. Kornack, J. C. Allred, and M. V. Romalis, A subfemtotesla multichannel atomic magnetometer, Nature **422**, 596 (2003).

[12] S. Pustelny, L. Busaite, M. Auzinsh, A. Akulshin, N. Leefer, and D. Budker, Nonlinear magneto-optical rotation in rubidium vapor excited with blue light, Phys. Rev. A **92**, 053410 (2015).

[13] P. D. D. Schwindt, S. Knappe, V. Shah, L. Hollberg, J. Kitching, L. A. Liew, and J. Moreland, Chip-scale atomic magnetometer, Appl. Phys. Lett. **85**, 6409 (2004).

[14] T. F. Cutler, W. J. Hamlyn, J. Renger, K. A. Whittaker, D. Pizzey, I. G. Hughes, V. Sandoghdar, and C. S. Adams, Nano-Structured Alkali-Metal Vapor Cells, Phys. Rev. Appl. **14**, 034054 (2020).

[15] S. Briaudeau, S. Saltiel, G. Nienhuis, D. Bloch, and M. Ducloy, Coherent Doppler narrowing in a thin vapor cell: Observation of the dicke regime in the optical domain, Phys. Rev. A - At. Mol. Opt. Phys. **57**, R3169 (1998).

[16] J. Keaveney, A. Sargsyan, U. Krohn, I. G. Hughes, D. Sarkisyan, and C. S. Adams, Cooperative Lamb Shift in an Atomic Vapor Layer of Nanometer Thickness, Phys. Rev. Lett. **108**, 1 (2012).

[17] S. Briaudeau, D. Bloch, and M. Ducloy, Detection of slow atoms in laser spectroscopy of a thin vapor film, Europhys. Lett. **35**, 337 (1996).

[18] S. J. Seltzer, et al., Investigation of antirelaxation coatings for alkali-metal vapor cells using surface science techniques, J. Chem. Phys. **133**, 144703 (2010).

[19] W. Yang, D. B. Conkey, B. Wu, D. Yin, A. R. Hawkins, and H. Schmidt, Atomic spectroscopy on a chip, Nat. Photonics **1**, 331 (2007).

[20] V. Shah, S. Knappe, P. D. D. Schwindt, and J. Kitching, Subpicotesla atomic magnetometry with a microfabricated vapour cell, Nat. Photonics **1**, 649 (2007).

[21] S. Groeger, G. Bison, J. L. Schenker, R. Wynands, and A. Weis, A high-sensitivity laser-pumped Mx magnetometer, Eur. Phys. J. D **38**, 239 (2006).

[22] V. Jacques, B. Hingant, A. Allafort, M. Pigeard, and J. F. Roch, Nonlinear spectroscopy of rubidium: An undergraduate experiment, Eur. J. Phys. **30**, 921 (2009).

[23] P. Siddons, C. S. Adams, C. Ge, and I. G. Hughes, Absolute absorption on rubidium D lines: Comparison between theory and experiment, J. Phys. B At. Mol. Opt. Phys. **41**, 155004 (2008).

[24] S. Tsvetkov, M. Taslakov, and S. Gateva, Dynamics of the light-induced atomic desorption at homogeneous illumination, Appl. Phys. B **123**, 92 (2017).

[25] E. Mariotti, S. Atutov, M. Meucci, P. Bicchi, C. Marinelli, and L. Moi, Dynamics of rubidium light-induced atom desorption (LIAD), Chem. Phys. **187**, 111 (1994).

[26] M. Meucci, E. Mariotti, P. Bicchi, C. Marinelli, and L. Moi, Light-induced atom desorption, Europhys. Lett. **25**, 639 (1994).

[27] K. Rębilas, Light-induced atomic desorption dynamics: Theory for a completely illuminated cell, Phys. Rev. A **80**, 014901 (2009).

[28] S. Pustelny, V. Schultze, T. Scholtes, and D. Budker, Dichroic atomic vapor laser lock with multi-gigahertz stabilization range, Rev. Sci. Instrum. **87**, 063107 (2016).

[29] C. Lee, G. Z. Iwata, E. Corsini, J. M. Higbie, S. Knappe, M. P. Ledbetter, and D. Budker, Small-sized dichroic atomic vapor laser lock, Rev. Sci. Instrum. **82**, 043107 (2011).

[30] M. A. Perez, U. Nguyen, S. Knappe, E. Donley, J. Kitching, and A. M. Shkel, in Proceedings of the IEEE International Conference on Micro Electro Mechanical Systems (MEMS) (2008).

[31] C. Klempt, T. van Zoest, T. Henninger, O. Topic, E. Rasel, W. Ertmer, and J. Arlt, Ultraviolet light-induced atom desorption for large rubidium and potassium magneto-optical traps, Phys. Rev. A **73**, 013410 (2006).

[32] J. H. Xu, A. Gozzini, F. Mango, G. Alzetta, and R. A. Bernheim, Photoatomic effect: Light-induced ejection of Na and Na_2 from polydimethylsiloxane surfaces, Phys. Rev. A **54**, 3146 (1996).

[33] S. N. Atutov, V. Biancalana, P. Bicchi, C. Marinelli, E. Mariotti, M. Meucci, A. Nagel, K. A. Nasyrov, S. Rachini, and L. Moi, Light-induced diffusion and desorption of alkali metals in a siloxane film: Theory and experiment, Phys. Rev. A **60**, 4693 (1999).

[34] See the Supplemental Material at http://link.aps.org/supplemental/10.1103/PhysRevApplied.15.L051001 for the effect of temperature on the optical isolator and DVALL lineshape calculations.

[35] E. Brekke and N. Swan, Saturation and alternate pathways in four-wave mixing in rubidium, J. Opt. Soc. Am. B **36**, 421 (2019).

[36] D. J. Whiting, R. S. Mathew, J. Keaveney, C. S. Adams, and I. G. Hughes, Four-wave mixing in a non-degenerate four-level diamond configuration in the hyperfine paschen–back regime, J. Mod. Opt. **65**, 713 (2018).